Path-integral study of positronium decay in xenon

Terrence L. Reese
Southern University, Baton Rouge, Louisiana 70126

Bruce N. Miller
Texas Christian University, Fort Worth, Texas 76119

(Received 18 January 2001; published 20 November 2001)

We use path-integral Monte Carlo to study the properties of a quantum particle equilibrated in a classical Lennard-Jones fluid. By choosing $2m_e$ for its mass, and potential parameters corresponding to xenon, we are able to model the behavior of thermalized positronium above the xenon critical temperature. We carefully study the local distortion of the fluid in the neighborhood of the quantum particle, and use this information to compute the annihilation rate as a function of density on two isotherms. The results compare favorably with experiment below the critical point density. Contrary to accepted views, we demonstrate that positronium remains in a self-trapped state at over twice the critical point density.

DOI: 10.1103/PhysRevE.64.061201 PACS number(s): 61.20.−p

I. INTRODUCTION

The generic model consisting of a low-mass particle in thermal equilibrium with a simple fluid encompasses a range of interesting phenomena, including electron transport and positron and positronium decay [1,2,3,4]. It has been known for some time that gross changes in the electron mobility [5,6] or the positron lifetime [7] may accompany relatively small changes in fluid density in a large neighborhood of the liquid-vapor critical point. Theorists have modeled these systems using variants of mean-field theory [8] and Feynman's polaron approximation [9]. Experimental measurements of the orthopositronium pickoff decay rate are of special interest because they provide direct information concerning the local environment of the equilibrated quantum particle [10]. The purpose of this study is to investigate the properties of positronium in thermal equilibrium in xenon fluid. We are particularly interested in the dependence of the positron annihilation rate on the fluid density and temperature that, in turn, strongly depends on the positronium-atom correlation in position. The former may be measured experimentally [11,12] while the latter may be computed from first principles using the path-integral Monte Carlo (PIMC) technique [10]. Since positronium has a small mass, it must be modeled as a quantum particle, while for typical temperatures and densities, the fluid atoms may be treated classically. Because of the Fermionic repulsion between the electron in Ps and those identified with the fluid atoms, the Ps-atom scattering length is positive and the net Ps-atom interaction is repulsive [8]. Consequently, as the temperature is lowered, the fluid tends to avoid the Ps atom, resulting in a reduction of the annihilation rate below that predicted for the uncorrelated system, due to the reduced availability of atomic electrons for ''pickoff'' annihilation.

Nearly a decade ago we applied mean-field theory (MFT) [13,14] to the problem of predicting the annihilation rate of orthopositronium in a dense fluid. Following standard arguments [8], we assumed that the fluid acts as a continuous source of potential energy for the positronium. In MFT, the system takes the form of two interacting fluids consisting of the local fluid density and the square of the translational Ps wave function. The equilibrium constraint of minimum free energy or, equivalently, constant chemical potential, reduces the problem to a single nonlinear Schrödinger equation for the translational Ps wave function that may be solved numerically with the equation of state of the pure fluid as input. It was shown some time ago that MFT successfully predicts the annihilation rate of both positrons and positronium in equilibrium in dense helium gas near the critical temperature [15]. However, in gases with higher-critical temperatures, we found that the density dependence of the annihilation rate is badly misrepresented by the theory [13,14]. We suspected that the source of the problem was the presence of large density fluctuations in the fluid in the critical region. To account for these fluctuations, we abandoned the continuous fluid model and, instead, employed a hybrid statistical model in which classical atoms interact with the elements of a discretized, Feynman-Kac, path integral [16,17] representing the Ps atom. It had been shown earlier that the annihilation rate could be expressed in terms of the Ps-atom radial distribution function [10]. This was computed in the hybrid model using a Metropolis Monte Carlo algorithm [18,19].

PIMC places heavy demands on the computing environment. Confidence in the results requires obtaining convergence in both the number of samples and the ''size'' of the discretized path. The PIMC algorithm we employed stretched the available computing power for that time frame. Xenon was selected for the model atomic system because experimental measurements existed over a wide range of density [11]. In addition, the critical temperature is relatively high (289 K), placing a workable upper bound on the thermal wavelength for carrying out PIMC. Although significant blocks of CPU time were obtained on NSF Cray supercomputers, there was always some doubt as to the degree of convergence obtained. In the case of the Ps annihilation rate, although the density dependence crudely agreed with our expectations, there were apparent anomalies that could not be explained [17]. The purpose of this paper is to revisit those computations using modern technology to determine the source of the anomalies and to study the system behavior

at higher densities than was previously possible. In particular, we want to investigate whether the agreement with experiment may be improved using the existing microscopic model. The organization of the paper is as follows: In Sec. II, we describe the physical system. In Sec. III, we introduce the algorithm for carrying out path-integral Monte Carlo (PIMC) for the hybrid system. Results are presented in Sec. IV and discussed in Sec. V, along with our final conclusions.

II. PHYSICAL SYSTEM

A positron injected into a fluid from a radioactive source, such as Na^{22}, will rapidly thermalize. The positron may remain independent or it may combine with an electron in the fluid and form positronium. Positronium is available in two spin states, ortho (triplet) and para (singlet). The extra unit of angular momentum contained in the ortho state forbids the two gamma decay process, resulting in a much longer lifetime for the triplet state (140 nsec for *o*-Ps vs 1.2 nsec for *p*-Ps). A consequence is that the main method of *o*-Ps decay in a typical fluid arises from the annihilation of the positron with a valence electron from one of the fluid molecules via the two-gamma process instead of with its partner. This is known as pickoff decay. It is responsible for the long-lived component of the annihilation spectra [8].

Experimentally, the lifetime of an individual positron is determined by measuring the time between its formation and its destruction in the medium. For a Na^{22} positron source, the ejection of the positron from the nucleus occurs simultaneously with the release of a 1.28 MeV γ ray, which may be easily detected. Its destruction in the host medium is signaled by the detection of two 0.511 MeV photons. The rate of positron creation is sufficiently low that only one positron is present in the fluid at a time. A complete experiment consists of measuring the decay time of a large number of injected positrons (about 10^6) and constructing a histogram of the results (frequency vs time). The histogram may be considered to consist of two portions, ''early'' and ''late.'' The early part represents the decay of nonthermalized positrons and parapositronium and usually ends after approximately 7 nsec. The late part deals with the decay of free positrons and orthopositronium atoms, and may be modeled as a sum of two exponentials ($Ae^{-\lambda_1 t}+Be^{-\lambda_2 t}$). The terms λ_1 and λ_2 are the average decay rate of the free positrons and the average pickoff decay rate of orthopositronium atoms, respectively. In the following, λ will be understood to represent the average pickoff decay rate of orthopositronium [20].

Near room temperature, the Ps atom has a thermal wavelength much greater than the mean separation between the fluid molecules, effectively allowing it to interact with numerous fluid atoms simultaneously. The neutrality of the Ps atom and the fluid molecules leads to a weak polarization attraction between them at distances greater than a few angstroms. However, the fermionic repulsion between the electron of the Ps atom and the electrons of the fluid atoms (or molecules) results in a strong short-range repulsive force. The combination of the large thermal wavelength and the short-range repulsion means that the Ps atom will attempt to decrease its interaction potential energy by creating a volume of decreased fluid density within its vicinity.

The volume of altered fluid density is referred to as a ''bubble,'' and we may gain some insight by thinking about it as a macroscopic object. Over regions of temperature and average fluid density where the decrease in potential energy caused by the formation of the bubble is greater than the pressure-volume work needed to create it, the bubble will become stable and the Ps atom will become localized within it. This process is called self trapping because it is initiated by the presence of the Ps atom. The formation of a self-trapped state will decrease the density of valence electrons within the vicinity of the Ps atom and thus decrease its probability of annihilation.

Xenon is interesting to positron experimentalists because the large atomic polarizability anomalously enhances the free-positron annihilation rate. It is of interest for positronium studies because the critical temperature (289 K) is near room temperature and among the highest for a noble gas. Thus, the critical region is experimentally accessible. In addition, due to the relatively short thermal wavelength, it is more easily modeled with PIMC. Experiments measuring the decay rate of Ps in xenon at various densities on two isotherms (300 and 340 K) have been carried out by Toumisaari *et al.* [11]. They found that the *o*-Ps decay rate depends linearly on the average fluid density at very low densities for both temperatures. However, as the density is increased, the decay rate fails to keep up with the linear extrapolation on each isotherm. The deviation from linearity is greater at 300 K. In fact, near the critical density, the decay rate of the 300 K isotherm becomes nearly constant. Experiments on *o*-Ps decay in Ethane for a larger set of temperatures have shown that, as the critical temperature is approached, the deviations from linearity become more pronounced, and the region of constant decay rate near the critical density increases [21]. This is explained qualitatively by the observation that, in the critical region, the compressibility of the fluid is large so very little energy is required to create the bubble state. As the density continues to increase, the repulsion between the fluid molecules overwhelms the quantum repulsion between the Ps atom and the fluid molecules, and the bubble collapses. Thus, plots of the measured values of the pickoff decay rate of *o*-Ps versus density provide information concerning the microscopic environment in the vicinity of the Ps atom. The goal of this study is to explore the quantitative features of the Ps-xenon system using PIMC.

III. MODEL

A. Path-Integral Monte Carlo

Here, we describe the model and techniques we use to simulate the Ps-xenon system. The small mass of the Ps atom requires that its translational degrees of freedom be treated by quantum mechanics. Conversely, since the thermal wavelength of the fluid atoms for the two temperatures considered is less than an angstrom, their translational degrees of freedom will be treated classically. This hybrid representation is known as the *adiabatic* approximation. It eliminates the quantum features of the fluid molecules, and thus greatly reduces the complexity of the system. Since it is a micro-

scopic model, it automatically includes both density fluctuations of the atoms and quantum fluctuations of the light particle (in this case *o*-Ps). In previous work [22,17,23], it has been shown that the adiabatic approximation is able to qualitatively recreate many of the features of the Ps-xenon and e^+-xenon systems.

The partition function for the Ps-xenon system in the adiabatic approximation is given by

$$Z=(1/\Lambda^{3N}N!)\int d\underline{\mathbf{R}}e^{-\beta U(\underline{\mathbf{R}})}\mathrm{Tr}\{e^{-\beta\hat{H}}\}, \tag{1}$$

where $\underline{\mathbf{R}}$ represents the set of vector positions, $\underline{\mathbf{R}}_j$, of the N fluid atoms (or molecules), $U(\underline{\mathbf{R}})$ is the total fluid interatomic potential, and Λ is the atomic thermal wavelength. The trace is carried out over the position states of the Ps atom. The Hamiltonian operator $\hat{H}$ is the sum of the kinetic-energy operator and the interaction potential energy between Ps and the fluid atoms. Assuming that the interaction potential may be represented as a sum of two-particle, distance-dependent, terms, then the Ps Hamiltonian may be written as

$$\hat{H}=\hat{p}^2/2m+\sum_{j=1}^{N}V(|\mathbf{R}_j-\mathbf{r}|), \tag{2}$$

where $V(|\mathbf{R}_j-\mathbf{r}|)$ is the interaction potential between the Ps atom at $\mathbf{r}$ and a fluid atom at position $\mathbf{R}_j$, and m is the mass of the Ps atom. In the canonical ensemble, the average value of any quantity $\langle O\rangle$ is determined from

$$\langle O\rangle=\int d\underline{\mathbf{R}}e^{-\beta U(\underline{\mathbf{R}})}\mathrm{Tr}\{e^{-\beta\hat{H}}O\}/Z(\Lambda^{3N}N!). \tag{3}$$

Standard computational techniques that treat the Ps atom as a classical sphere do not result in the formation of a bubble, because they fail to include the Ps atom's quantum nature. However, the path-integral formulation was created to handle this problem [24,9,4,25,26]. Asserting the Trotter formula and inserting $p-1$ intermediate states between the exponentials, the Feynman discretized path-integral representation is obtained,

$$\langle\mathbf{r}|e^{-\beta\hat{H}}|\mathbf{r}\rangle=\prod_{i=0}^{p-1}[2\pi/\kappa^2]^{3/2}\int d\mathbf{r}_i e^{-p|\mathbf{r}_i-\mathbf{r}_{r+1}|^2/(2\kappa^2)}\times\rho(\mathbf{r}_i,\mathbf{r}_{r+1},\underline{\mathbf{R}};\varepsilon), \tag{4}$$

where $p-1$ is the number of intermediate Ps states, $\kappa^2=\hbar^2\beta/m$, and $\varepsilon=\beta/p$. The $\mathbf{r}_i$'s represent the positions of the Ps atom at intermediate imaginary times along the discretized path, while $\rho(\mathbf{r}_i,\mathbf{r}_{i+1},\underline{\mathbf{R}};\varepsilon)$ is the Boltzmann weighting factor determined by the interaction potential with the fluid molecules for the r_i and $\mathbf{r}_{i+1}$ pseudoparticles. The state $\mathbf{r}_p$ is the same as $\mathbf{r}_0=\mathbf{r}_0$.

The path-integral representation is similar to the partition function for a closed polymer chain consisting of p classical ''pseudo particles.'' This correspondence between the quantum representation of a single particle and the classical polymer is known as the classical isomorphism. It is important because, with it, the extensive statistical techniques used to study classical systems may also be used to compute the average properties of a quantum system. The quantum spread of the Ps atom is represented in the classical system by the finite spread of the polymer chain. In this formalism, states are represented by points in the $3(p+N)$-dimensional configuration space of the polymer-atom system.

Because of the two types of interaction, the distribution function cannot be sampled directly. Therefore, we must employ some version of the metropolis sampling algorithm (MSA) [18] as follows: An initial configuration for the system is created and its energy is computed. The only restraint on the initial configuration is that there is no overlap between the polymer particles and the fluid molecules. Trial configurations for the polymer and fluid molecules are created and their energy is computed. If the ratio of the statistical weight of the trial configuration and the previous configuration is greater than a random number between zero and one, then the trial configuration is acceptable and its configuration is used to determine the average value of the desired quantities. On the other hand, if the ratio is less than this random number, then the trial configuration is discarded and the previous configuration is again used to compute the averages.

The standard MSA creates trial configurations by moving a single particle and then determining its acceptability. While we use it to create positions for the fluid molecules, using the identical procedure for the polymer would not permit the effective exploration of the polymer's configuration space, and thus, we would obtain untrustworthy results. In our modified version of the MSA, a subchain containing n particles is formed out of the full polymer chain and trial positions are created for the particles on that subchain. The greater the number of particles on the subchain, the more rapidly the configuration space may be explored. The configuration space can be most rapidly explored if a new chain is created at every pass. However, because of the high percentage of rejections due to overlap between the polymer particles and fluid molecules, this method would be extremely inefficient. The number of particles on a subchain must be large enough to effectively explore the configuration space and small enough to avoid a high rejection rate from unacceptable polymer-fluid configurations. In practice, it was determined that the most efficient value of n for the segment is about 10% of the total number of pseudoparticles.

After a trial configuration has been created for a subchain and its acceptability determined, a subchain is created for which the first particle is located at the midpoint of the previous subchain. Other subchains are created in this ''leap-frog'' manner until the entire chain has been traversed. This method allows for effective sampling of the configuration space with a minimum of CPU time. After an attempt has been made to find another position for each polymer particle and fluid molecule, the definition of a pass, this configuration is used to compute the value of the physical quantities of interest. The process is repeated until the averages converge.

B. Potential

The most important factor in determining the acceptance of a trial configuration is its interaction potential energy with

the other particles in the system. The strong short-range repulsion and the very weak interaction at larger distances between Ps and xenon will be represented by a hard-sphere-type approximation with closest distance of approach $R_{\rm hs}$. If the distance between any of the particles on a subchain and one of the fluid molecules is less than $R_{\rm hs}$ then that trial subchain is rejected. The same situation also applies for trial positions of the fluid molecules that overlap with polymer particles. This standard hard-sphere potential is known as the primitive approximation.

The accuracy of the path-integral approximation is dependent upon the value of p, which is strongly related to how rapidly the interaction potential changes. The value of p should be large enough that adjacent particles on the chain do not feel different potentials. Thus, the greater the potential gradient, the more particles that are required on the chain. Because of the discontinuity in potential energy at $R_{\rm hs}$, in the primitive approximation the value of p should approach infinity near this value. Barker devised the image approximation to the hard-sphere potential to overcome this difficulty [27]. It smooths the discontinuity at $R_{\rm hs}$, reducing the number of polymer particles necessary for convergence. In these computations, we will use the version devised by Whitlock and Kalos [28] where

$$\rho(\mathbf{r},\mathbf{r}',\mathbf{R}_j,\epsilon)=1-e^{-2pF(\mathbf{r},\mathbf{r}',\mathbf{R}_j)} \tag{5}$$

if $|\mathbf{r}-\mathbf{R}_j|$ and $|\mathbf{r}'-\mathbf{R}_j|$ are greater than $R_{\rm hs}$ and $\rho(\mathbf{r},\mathbf{r}',\mathbf{R}_j,\epsilon)=0$ otherwise. In the above

$$F(\mathbf{r},\mathbf{r}',\mathbf{R}_j)=(|\mathbf{r}-\mathbf{R}_j|^2-R_{\rm hs}^2)(|\mathbf{r}'-\mathbf{R}_j|^2-R_{\rm hs}^2)/(\Lambda_{\rm Ps}^2R_{\rm hs}^2), \tag{6}$$

$\Lambda_{\rm Ps}=\sqrt{\hbar^2\beta/m}$ is the thermal wavelength of positronium and $|\mathbf{r}-\mathbf{R}_j|$ and $|\mathbf{r}'-\mathbf{R}_j|$ are the distances between fluid molecule $\mathbf{R}_j$ and the polymer particles at $\mathbf{r}$ and $\mathbf{r}'$. This choice decreases toward zero more rapidly than the one used by Barker. Thus, it more accurately models the hard-sphere potential. The interaction between the fluid molecules is represented by the standard Lennard-Jones 6–12 potential and the standard MSA is used to compute the properties of the fluid interaction.

C. Important quantities

1. Structural quantities

The polymer-fluid radial distribution function,

$$g_{\rm fp}(r)=\left\langle \sum_{j=1}^{N}\sum_{i=0}^{p-1}\delta(\mathbf{R}_j-\mathbf{r}_i-\mathbf{r})/p\right\rangle \Big/ \rho, \tag{7}$$

determines the density of fluid molecules around each polymer particle. It is important because it is used to directly compute the average decay rate. Information concerning the density of fluid molecules around the center of mass of the polymer is given by

$$g_{fc}(r)=\left\langle \sum_{j=1}^{N}\delta(\mathbf{R}_j-\mathbf{r}_{\rm cm}-r)\right\rangle \Big/ \rho, \tag{8}$$

where $\mathbf{r}_{\rm cm}$ is the position of the geometric center of mass of the polymer chain and $r=|\mathbf{r}|$. It is useful for determining the presence of a self-trapped state. In an extended state, the density differs from zero close to the center of mass. A nonzero density at the center of mass has already been observed with PIMC for very low densities [17,26]. A self-trapped state is distinguished by the exclusion of fluid molecules away from the polymer center of mass. The physical properties of the fluid may be determined from the fluid-fluid radial distribution function:

$$g_{\rm ff}(R)=\left\langle \sum_{i>j=1}^{N}\delta(\mathbf{R}_i-\mathbf{R}_j-\mathbf{R})\right\rangle, \tag{9}$$

where $R=|\mathbf{R}|$.

The mean density of polymer particles at a distance r from the polymer center of mass

$$g_{\rm pc}(r)=\left\langle \sum_{i=0}^{p-1}\delta(\mathbf{r}_i-\mathbf{r}_{\rm cm}-\mathbf{r})\right\rangle \tag{10}$$

is the probability density of the Ps atom. This quantity is also an indicator of the formation of a self-trapped state. The polymer particles are more confined near the center of mass in a self-trapped state. Since the decay rate depends upon the overlap between the portion of the positron wave function beyond $R_{\rm hs}$ and the density of fluid electrons of opposite spin, the more confined the polymer, the lower the probability of an encounter between a polymer particle and a fluid molecule.

Information concerning the behavior of the polymer may also be determined from the root mean-square displacement (RMSD) $\sqrt{\langle|\mathbf{r}(t)-\mathbf{r}'(t')|^2\rangle}$ between two particles on the chain separated by the imaginary time interval, $0\leqslant(t-t')\leqslant\beta\hbar$. It may be calculated analytically for a free particle in the absence of the fluid [26],

$$\langle|\mathbf{r}(t)-\mathbf{r}'(t')|^2\rangle=3\Lambda_{\rm Ps}^2(t-t')[\beta\hbar-(t-t')]/(\beta\hbar)^2. \tag{11}$$

Plots of the RMSD versus $(t-t')$ provide a measure of the degree of localization of the polymer. For a free particle, or an extended state, the shape of the plot is an inverted Gaussian with a strong central maximum at $t-t'=\beta\hbar/2=p/2$. As the average density of the fluid is increased, the Gaussian becomes flattened until, in a completely self-trapped state, the RMSD is constant except near the ends.

2. Decay rate

The decay rate is the only quantity that was directly measured in the experiments mentioned above [11]. In the adiabatic approximation, the average decay rate of the Ps atom in xenon is

$$\langle\hat{\lambda}\rangle=\int d\underline{\mathbf{R}}e^{-\beta U(\underline{\mathbf{R}})}{\rm Tr}\{e^{-\beta\hat{H}}\hat{\lambda}\}/Z(\Lambda^{3N}N!), \tag{12}$$

where $\hat{\lambda}$, the instantaneous decay rate operator, is given by

$$\hat{\lambda} = \sum_{j=1}^{N} f(\mathbf{R}_j - \mathbf{r}_+). \tag{13}$$

It must be remembered that Ps is a composite particle, so in calculations of the decay rate it is the position of the positron that is important. In this case, the trace must be carried out over the states available to the positron. In Eq. (13) $f(\mathbf{R}')$ is the electron charge distribution at a displacement $\mathbf{R}'$ from the atom and r_+ is the position of the positron. Assuming that Ps is in the ground state and writing $\boldsymbol{\omega} = \mathbf{r}_+ - r_-$, we easily obtain

$$\langle \hat{\lambda} \rangle = [\rho/(8\pi a_0^2)] \int dR' \times \int d\boldsymbol{\omega} f(|\mathbf{R}' - \boldsymbol{\omega}|2) e^{-\omega/a_0} g_{fp}(R'), \tag{14}$$

where $\mathbf{R}'$ is the vector distance between a polymer particle and a fluid molecule, $R' = |\mathbf{R}'|$ and ρ is the average fluid density. The average decay rate is thus seen to be dependent upon the polymer-fluid radial distribution function. For a more detailed derivation, see Reese and Miller [17]. In our calculations, we assumed that the electronic charge density of the molecules is a delta function centered on the atomic nucleus. Although this approximation is naive, it recreates many of the qualitative properties of the system. In this approximation, the decay rate is the overlap between that part of the positron wave function that manages to leak beyond R_{hs} and the coordinates of the atomic nuclei

$$\langle \hat{\lambda} \rangle = \rho/(\pi a_0^3) \int dR' e^{-2R'/a_0} g(R'). \tag{15}$$

If the hard-sphere diameter is too large, then the fluid molecules are too far away to overlap with the positron wave function. On the other hand, if the hard-sphere diameter is too small then too much of the positron wave function leaks beyond R_{hs} and the overlap becomes constant and independent of the fluid density. A value for the effective hard-sphere diameter was determined by computing the ratio of the decay rate from the experimental results at 1/20th the critical density and at the critical density to the values of the linear extrapolation (see Sec. II above) at these densities for the 340 K isotherm [11]. Monte Carlo calculations of the decay rate were computed at these densities for selected values of R_{hs}.

It was determined that the results closest to the experimental data were obtained for hard-sphere diameters of 2 and 2.5 Å. In the following, the hard-sphere diameter was simply assigned the average value of 2.25 Å.

3. Algorithm

In the calculations reported in this paper, a Monte Carlo algorithm was employed that explores the configuration space as effectively as the staging method used earlier [17,25] but is less complicated to implement, and faster. The algorithm depends on four parameters: Λ_{Ps}, the Ps thermal wavelength, σ, the Lennard-Jones distance parameter, ρ^* $(=\rho\sigma^3)$, the scaled average density of the fluid, and R_{hs}, the hard-sphere diameter, and operates as follows: First an initial configuration is created for the entire system. The center of mass of the initial polymer is located at the center of a cube of side $3\Lambda_{\mathrm{Ps}}$. The fluid atoms are then created randomly in the cube with the only constraint that they do not overlap with the hard-sphere excluded volume generated by the polymer. The number of fluid molecules is determined by the average density of the fluid, $N = \rho V$. To minimize size effects, the edge of the cube was selected to be greater than three times the thermal wavelength of the Ps atom. The energy of this initial configuration is then computed.

Configurations for the polymer are generated by moving chain segments of length *n*. A normal modes scheme was devised to create trial positions for the particles on the subchain segments. The potential energy for this trial segment is then computed using the image approximation. If it is accepted, then it replaces the previous segment. The leap frog method is then used to create a trial subchain and the process is repeated until a new position has been attempted for every particle on the chain.

After the polymer chain has been completely ''regrown,'' trial positions for the fluid molecules are created by translating the original coordinates by a displacement that is equal to the product of the mean separation between the fluid molecules and a random number in the unit interval. The acceptance of this position is determined using the standard MSA. After an attempt has been made to move every particle at least once, the resulting configuration is then used to compute values of the physical quantities of interest. The acceptance for trial positions of the fluid molecules should be between 40 and 60% to allow for efficient sampling. Because at higher densities using the mean separation between fluid molecules as a translation factor may lead to a very low-acceptance rate, a routine was created that would reduce this factor to increase the acceptance rate if it fell below 40%.

Like the staging method, this algorithm is highly amenable to vectorization because the position of particles on the subchains is dependent only upon the end points. In addition, the algorithm is readily parallelized. The number of passes required for convergence may be split among different processors and the results averaged together at the end. It is also highly stable from platform to platform because of its low reliance on specialized subroutine calls.

IV. RESULTS

A. Convergence

The goal of this paper is to determine if the path-integral Monte Carlo technique using the simple image approximation and the delta function charge distribution is capable of simulating the gross properties of the Ps-xenon system. The calculations were made using six density values ($\rho^* = 0.017$, 0.035, 0.088, 0.17, 0.3, 0.35, 0.4, and 0.7) on each isotherm. These points were selected because they span a range from the dilute vapor phase to twice the experimental critical density. The tabulated parameters we employed in the Lennard-Jones potential to represent xenon are σ

$=4.0551$ Å and $\epsilon=229$ K [29]. The calculations were made at 300 and 340 K, the temperatures used in the experiments [11].

If the results of a calculation are valid, they should be independent of the number of fluid molecules, the number of particles on the polymer, and the number of passes through the system provided these numbers are sufficiently large. Stability with respect to increases in these parameters is called convergence. The determination of the number of passes required for convergence is accomplished by tracking the value of the root-mean-square displacement (RMSD) for the particle at $t=p/2$ and the average decay rate. When the averages cease to fluctuate in the third significant figure, then convergence is achieved. The two lowest densities required approximately 8000 passes to converge, which was longer than that of any of the other densities. In fact, the greater the density, the fewer the number of passes required for convergence. The number of passes for each density run was set to 10 000.

The appropriate value of p was determined by comparing the decay rates from calculations using increasing values of p. For densities lower than 0.17, test runs showed that a minimum of 500 particles are required on the chain and that 1000 particles are required for densities from 0.17 to 0.4. At a density of 0.7, 2000 particles are required. The final value of p for all calculations was set at 2000 so that all results could be compared together. The number of fluid molecules used was no less than 2000 in all calculations. However, in accordance with maintaining an edge length of no less than $3\Lambda_{\mathrm{Ps}}$, the number of fluid molecules at the critical density, $\rho^*=0.35$, and at $\rho^*=0.7$ was 3400 and 8000, respectively, at 300 K and was slightly less at 340 K.

Because of the lack of sufficient computing power, our original calculations [17] did not have a sufficient number of fluid atoms to meet the criteria that the sides of the cube must be $3\Lambda_{\mathrm{Ps}}$. The maximum number of fluid molecules that were used in those calculations was 500, leading to the possibility of inaccuracy because of finite-size effects. Also, in the previous calculations only four density points were used (0.017, 0.088, 0.17, and 0.35) to compute the equilibrium properties of the system due to the lack of computer resources.

B. Structural results

Figure 1 contains the plot of the RMSD versus polymer particle number $(t-t')$ at $T=300$ K for three density points. Even at very low densities, the polymer is slightly constrained by the fluid molecules, as can be seen by the fact that the low-density curve is slightly lower than that of the free polymer. As the density is increased, the curve becomes increasingly flattened, indicating that the spread of the polymer is becoming smaller. At the Lennard-Jones critical density, the RMSD curve is constant in the region $700<(t-t')<1300$, indicating that although the polymer is strongly constrained, it is not in a completely self-trapped state. Except near the end points, the RMSD curve is virtually constant for $\rho^*=0.7$. In this case, the polymer particles are nearly the same distance apart and strongly confined. The value at the midpoint is less than half of that of the free particle. This is the perfect example of a self-trapped state. RMSD plots for 340 K are similar. The experimental measurements of the annihilation rate at 300 K suggest that self trapping occurs over a density range [0.3, 0.4]. The failure of the polymer to achieve complete self trapping at the critical density may be due a too small choice of the hard-sphere diameter. An R_{hs} value closer to 2.5 Å would result in a more confined state for the polymer at the critical density.

Figures 2(a) and (b) are plots of the radial distribution function and the density of fluid molecules from the polymer center of mass, versus position for $T=300$ K. The plots of $g_{\mathrm{fp}}(r)$ begin to increase at the hard-sphere diameter at different rates, with $\rho^*=0.7$ having the most rapid increase. The critical density curve shows the slowest rate of increase, so at the same distance from the polymer particle, the density of fluid molecules at $\rho^*=0.35$ is much less than at the other two densities. Thus, the probability of annihilation for the positron is much smaller at the critical density. As in our original calculations, the critical density curve eventually increases beyond one, surpassing the lowest-density value before settling back to one. This indicates that just outside the range of the Ps atom's influence, fluid molecules begin to pile up. The large value of the high-density curve shows that while the polymer is more confined than at the critical density, the fluid molecules, despite the repulsive potential, congregate more closely at the edge of the polymer's influence than at the lower densities, thus increasing the probability of the positron's annihilation.

Figure 2(b) reinforces many of the features noticed in Fig. 2(a). Again, at the critical density fluid molecules are expelled more strongly than at the other densities. While curves for both $\rho^*=0.35$ and $\rho^*=0.7$ begin increasing just outside of the Lennard-Jones diameter, the high-density curve increases much faster. A stable bubble of radius slightly greater than 4 Å is easily seen on the plot for each density. As in the previous computations, the lowest-density curve is nonzero at the origin. Comparisons between the radial distribution functions here and the original runs show that although the curves have similar features, the older curves had a higher rate of increase than the newer ones. An interesting feature of the high-density plot is the oscillatory structure outside of the excluded trapping volume. Fluctuations play a smaller role here than at the critical density, and we can clearly see the arrangement of atoms in concentric shells about the center.

All of these plots were repeated at 340 K. For the sake of brevity we do not include them here, but simply remark that they are qualitatively similar to their 300 K cousins. In general, as a result of the greater pressure, the densities and distribution functions at 340 K increase towards their asymptotic value more rapidly than at 300 K.

C. Decay rate

An important goal of our simulation is to recreate the transition region in experimental measurements of the Ps pickoff decay rate. Computations of the decay rate using MFT contain a sharp discontinuity between the extended state and the self-trapped state, while experimental measure-

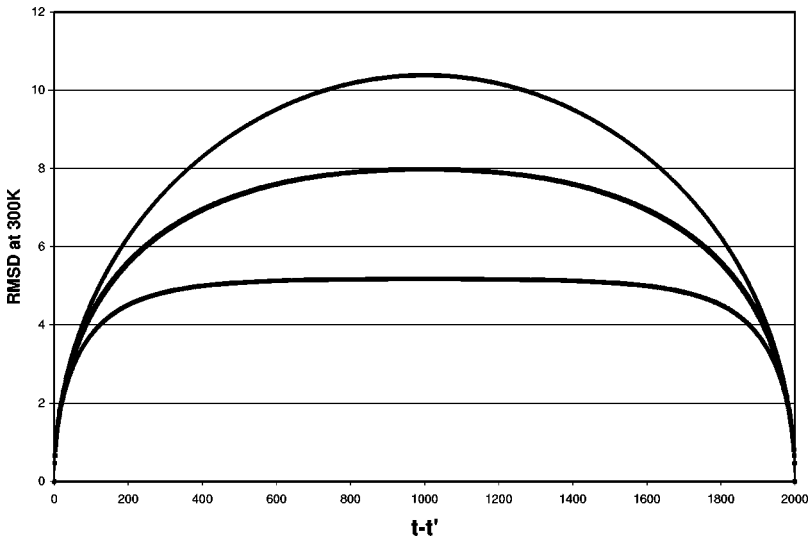

FIG. 1. Plot of the root-mean-square displacement $\langle|\mathbf{r}(t)-\mathbf{r}'(t')|^2\rangle^{1/2}$ (angstroms) versus $t-t'$, where t is an integer that labels the pseudoparticle on the discretized path at $T=300$ K. From top to bottom, the curves correspond to scaled densities $\rho^*=0.017$; 0.35; 0.7. At the lowest density, the quantum particle is nearly free while, at the highest density, it is strongly trapped.

ments show a gradual transition. MFT does not include density fluctuations, which can become important in the transition to a self-trapped state. Because the PIMC technique is based on a microscopic model, it automatically includes the fluctuations and was shown in previous computations not to have a discontinuity at the transition to self trapping [17]. These new calculations show improvement in mapping the transition region and, overall, a decay rate curve more closely resembling the experimental results. The techniques used in these computations of the decay rate in terms of $g_{\mathrm{fp}}(r)$ were the same as in our previous work, the important differences being many more fluid atoms and a hard-sphere diameter of 2.25 Å.

Figures 3(a) and (b) are plots of the decay rate versus ρ^* for $T=300$ and 340 K, respectively. Each plot contains the theoretical computations and the experimental results. The straight line in each curve is the linear extrapolation that represents the extension of the very low-density dependence of the decay rate. In both plots, the theoretical curves are close to the experimental results below the critical point density. For densities below $\rho^*=0.3$, the experimental decay rates are greater than the theoretical curves in both plots. However, slightly over $\rho^*=0.3$ the curves cross and the theoretical curves exceed the experimental results. In the region between $0.3<\rho^*<0.4$, the experimental plot at 300 K has virtually no slope, while a small but noticeable increase may be seen on the other isotherm. In this region, the theoretical curves suggest a less-defined trapped state than the experiments. There are also noticeable differences between the computed decay rates in the critical region, but they are more complex and suggest a less-defined trapped state than the experiments. This is confirmed by the RMSD (see above). In the original computations, the theoretical decay rate plots were linear and exhibited much less curvature than the new results.

The experimental plots stop at approximately $\rho^*=0.4$, slightly above the critical point density, at 340 K and 0.59 at 300 K. However, we continued the simulations to twice the critical density to investigate the region in which experiments on other fluids demonstrate that the decay rate rapidly increases [21]. It is clear from the figures that the simulations share this property. The results from the structural computations showed that although at this high density, the Ps atom is more confined than at the critical density, the high density of fluid molecules close to the positronium cause a large increase in the decay rate over that at the critical density. This is in contrast with MFT, which predicts a sudden collapse of the bubble above a critical value of the density. The computations confirm that the decay rate rapidly increases between $0.4<\rho^*<0.7$ at each temperature.

D. Fluctuations

The use of the Feynman-Kac path integral allows us to compute the fluctuations of physical quantities represented by operators which are C numbers in the position representation. The decay rate is such an operator. In the simulations reported here, it is straightforward to compute a decay rate value after each pass through the system, i.e., after each polymer is created. The mean decay rate is simply the average of this quantity over 10 000 passes following a period of annealing. Its variance may be constructed from the same data. In Fig. 4, we have plotted the dispersion (standard deviation/mean) of the decay rate versus density on each isotherm. We see that fluctuations are roughly 25% of the mean at low density, and decrease to less than 5% as the density is increased. Moreover, the behavior near the critical density is not remarkably different from the remainder of the data. This is in sharp contrast with our earlier studies using fewer fluid atoms, where the pattern was similar, but the magnitude of the fluctuations was of the same order as the mean at some densities [17,30]. Apparently, the large fluctuations reported earlier were due to size effects, rather than the anticipated large-density fluctuations of the fluid in the critical region [31].

V. SUMMARY AND CONCLUSIONS

The large thermal wavelength of a light particle (positron, electron, or positronium atom) leads to quantum effects that are impossible in the classical regime. Subatomic particles push around fluid atoms many times more massive than

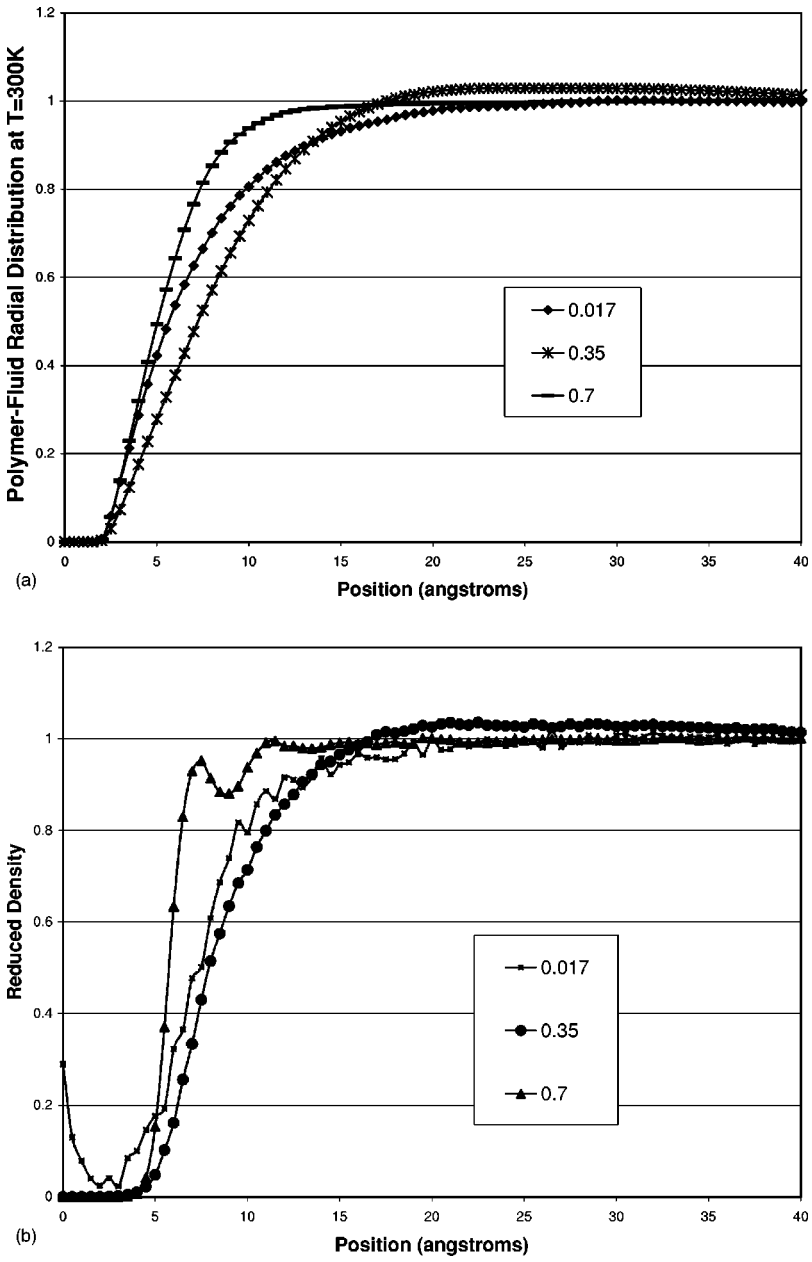

FIG. 2. (a) Plot of the polymer-fluid radial distribution function, $g_{\mathrm{fp}}(\mathbf{r})$, versus position at $T=300$ K. The scaled densities are $\rho^*=0.017$; 0.35; 0.7. (b) Plot of the reduced fluid density from the polymer center of mass, $g_{\mathrm{fc}}(\mathbf{r})$, versus position at $T=300$ K. The mean scaled densities are $\rho^*=0.017$; 0.35; 0.7.

themselves, creating anomalous behavior in properties that depend on the local density, such as the positron decay rate or, the electron mobility. An important goal of our investigations is to determine if the PIMC method is capable of accurately simulating the Ps-fluid system. As a first step, we have used the PIMC technique with a hard-sphere Ps-atom potential and delta function approximation for the atomic electron density to see if it can recreate the major features of the Ps-xenon system. Because it includes density fluctuations, the PIMC technique allows the transition regions to be investigated, in contrast with MFT, which predicts an artificial discontinuity at the transition between the extended and the trapped states.

The use of the adiabatic approximation in modeling the Ps-xenon system is justified because of the large difference in thermal wavelengths between the Ps atom and the fluid atoms. The classical isomorphism connects the partition functions of a classical closed polymer consisting of p pseudoparticles with the trace of the quantum-mechanical density matrix. This important step allows the use of classical Monte Carlo techniques to be applied in the computation of quantum-mechanical equilibrium averages, explicitly the pickoff decay rate.

The hard-sphere potential is used to represent the Ps-xenon interaction. Rapidly changing potentials require large number of polymer particles on the chain to accurately simulate them. This problem is compounded with the discontinuity at R_{hs} inherent in the hard-sphere potential that would lead to an infinite number of polymer particles. The image approximation to the hard-sphere potential is used to smooth out the discontinuity at the hard-sphere diameter and reduce p to a reasonable value. Because of the large value of p required for convergence, the standard MSA is incapable of adequately exploring the polymer configuration space. A

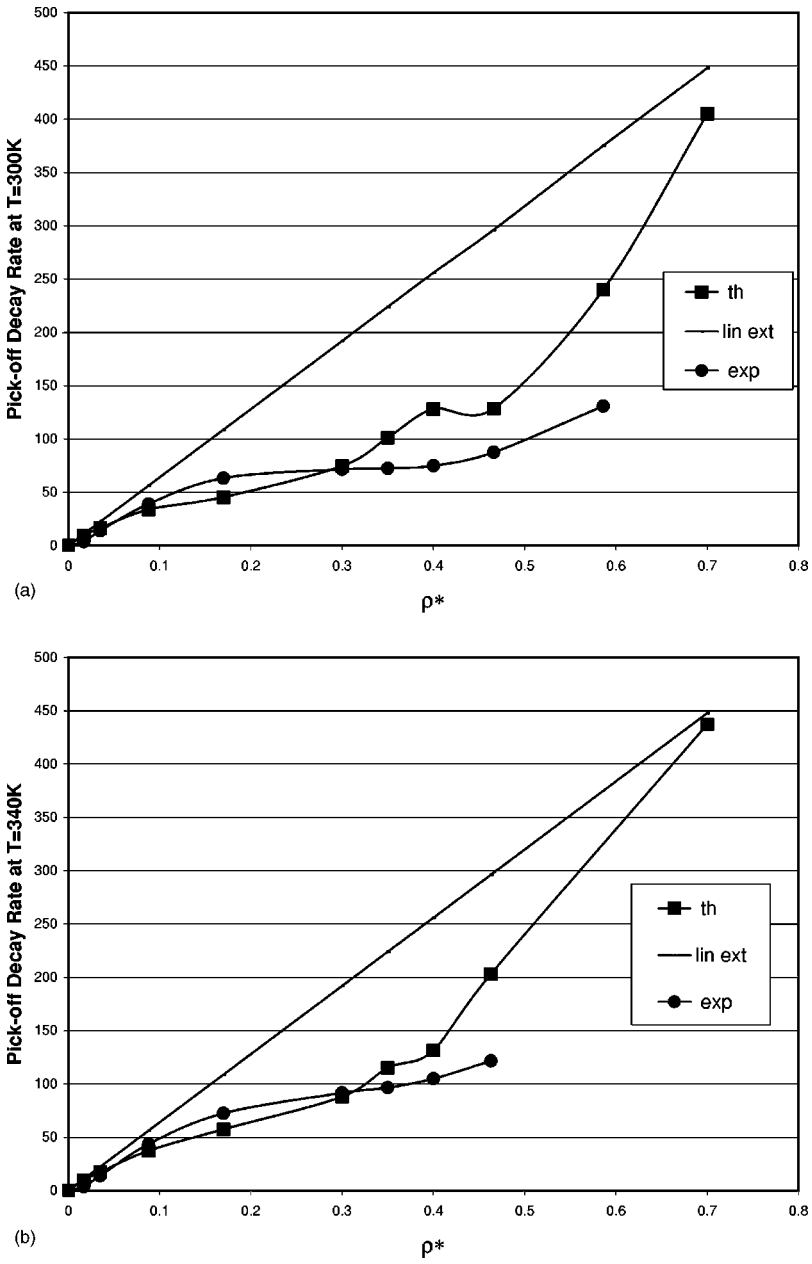

FIG. 3. (a) Plot of the pickoff decay rate versus scaled density at $T=300\,\mathrm{K}$ (in units of 10^6/sec). The straight line is the linear extrapolation of the low-density behavior. Both experimental (exp) and theoretical (th) curves are displayed. (b) Same as (a), but at $T=340\,\mathrm{K}$.

subchain consisting of n particles is used to overcome these difficulties. A trial configuration is created for the subchain and its energy is computed. The standard MSA is then used to determine the acceptability of the trial configuration for the subchain. The ''leapfrog'' method insures sufficiently ''ergodic'' sampling in a reasonable amount of CPU time.

In the original calculations, it was necessary to make a number of compromises with respect to convergence due to the lack of computer power. Those results showed that the PIMC technique had some of the properties of the Ps-xenon at low densities, however, the results near the critical density were suspect and nothing was known about the higher-density regions where MFT suggests that self trapping begins to fail. The computers used in the present studies have sufficient RAM to store atomic positions within a box of edge length of at least $3\Lambda_{\mathrm{Ps}}$, and enough speed to complete the computations in a reasonable amount of time. Structural quantities, like the RMSD and the radial distribution function, contain information on the state of the quantum particle and the environment around it. The other quantity of interest that is computed is the pickoff decay rate, which may be compared with experimental measurements.

The results of the RMSD computations show that, as the density is increased, the quantum particle becomes more confined. At the highest density, the distance between almost all of the pseudoparticles in the polymer representation is the same, indicating a completely self-trapped state. In the plots of the polymer-fluid radial distribution functions, as well as the density of fluid atoms from the polymer center of mass versus position, it is seen that at the critical density, the fluid molecules are expelled from the vicinity of the polymer. This results in the much smaller probability of annihilation of the positron observed in experiments. Mean-field theory suggests that well above the critical density, the decay rate re-

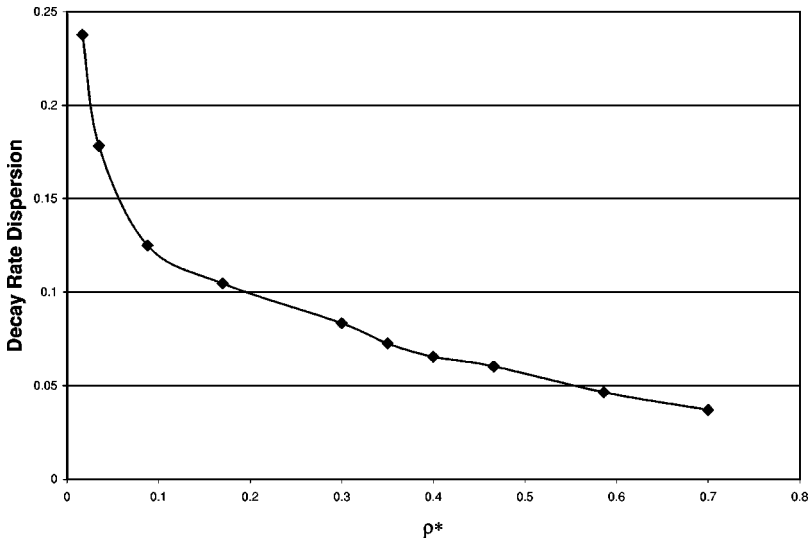

FIG. 4. Plot of the decay rate dispersion (standard deviation/average decay rate) versus scaled density at $T=300$ K.

turns to the predicted linear density dependence due to the collapse of the bubble. Here, we see that no such thing occurs. At the highest density value ($\rho^*=0.7$), it is noted that the large local density of fluid molecules at the edge of the bubble results in the increased probability of positron annihilation.

Compared to the earlier computations, the plots of the decay rate versus density now show curvature, sharing some of the attributes of the experimental curves. Both at 300 and 340 K, they also show the rapid, nonlinear, increase above the critical density seen in other experiments [21]. Unfortunately, there is no sufficient data available for xenon to compare with the simulations at these higher densities. However, on the 300 K isotherm near the critical density, the theoretical curve does not show a plateau and has a higher value than the experimental results. The 300 and 340 K theoretical isotherms have similar shapes: In particular, they both show an anomalous rise above the critical density that is not present in the experimental data. It will be interesting to determine if this is a consequence of either the simplified interaction potential or atomic electron density used to perform the simulations. Alternatively, the rise may be due to a finite-size effect resulting from a change in asymptotic density or pressure far from the quantum particle induced by the displacement of fluid atoms from the trap. This will be investigated in a future study.

ACKNOWLEDGMENTS

The authors are grateful for the support of the Department of Information Services at Texas Christian University and the Center for Computational Sciences at the University of Kentucky.

[1] J. Hernandez, Rev. Mod. Phys. **63**, 675 (1991).
[2] D. Chandler and K. Leung, Annu. Rev. Phys. Chem. **45**, 557 (1994).
[3] G. N. Chuev, Izv. Akad. Nauk, Ser. Fiz. **61**, 1770 (1997).
[4] B. J. Berne and D. Thirumali, Annu. Rev. Plant Physiol. **37**, 401 (1986).
[5] A. F. Borghesani and M. Santini, Phys. Rev. A **45**, 8803 (1992).
[6] N. Gee and G. R. Freeman, Can. J. Chem. **64**, 1810 (1986).
[7] P. Hautojarvi, K. Rytsola, P. Tuovinen, and P. Jauho, Phys. Lett. A **57**, 175 (1976).
[8] I. T. Iakubov and A. G. Khrapak, Rep. Prog. Phys. **45**, 697 (1982).
[9] A. L. Nichols III, D. Chandler, Y. Singh, and D. M. Richardson, J. Chem. Phys. **81**, 5109 (1984).
[10] B. N. Miller and Y. Fan, Phys. Rev. A **42**, 2228 (1990).
[11] M. Tuomisaari, K. Rytsola, and P. Hautojarvi, J. Phys. B **21**, 3917 (1988).
[12] T. J. Murphy and C. M. Surko, J. Phys. B **23**, L727 (1990).
[13] Bruce N. Miller and Terrence Reese, Phys. Rev. A **39**, 4735 (1989).
[14] Terrence Reese and Bruce N. Miller, Phys. Rev. A **42**, 6068 (1990).
[15] M. J. Stott and E. Zaremba, Phys. Rev. Lett. **38**, 1493 (1977).
[16] Richard P. Feynman, *Statistical Mechanics* (Addison-Wesley, Reading, MA, 1972).
[17] T. L. Reese and B. N. Miller, Phys. Rev. E **47**, 2581 (1993).
[18] N. Metropolis, A. W. Rosenbluth, M. N. Rosenbluth, A. H. Teller, and E. Teller, J. Chem. Phys. **21**, 1087 (1953).
[19] M. H. Kalos and P. A. Whitlock, *Monte Carlo Methods Volume I: Basics* (Wiley, New York, 1986).
[20] K. F. Canter, J. D. McNutt, and L. O. Roellig, Phys. Rev. A **12**, 375 (1975).
[21] S. C. Sharma (unpublished).
[22] G. A. Worrell and B. N. Miller, Phys. Rev. A **46**, 3380 (1992).
[23] Y. Fan and B. N. Miller, J. Chem. Phys. **93**, 4322 (1990).
[24] D. Chandler and P. G. Wolynes, J. Chem. Phys. **74**, 4078 (1981).

[25] M. Sprik, M. L. Klein, and D. Chandler, Phys. Rev. B **31**, 4234 (1985).
[26] D. F. Coker, B. J. Berne, and D. Thirumali, J. Chem. Phys. **86**, 5689 (1987).
[27] J. A. Barker, J. Chem. Phys. **70**, 2914 (1979).
[28] P. A. Whitlock and M. H. Kalos, J. Chem. Phys. **30**, 361 (1978).
[29] A. E. Sherwood and J. M. Prausnitz, J. Chem. Phys. **41**, 429 (1964).
[30] B. N. Miller, T. L. Reese, and G. Worrell, Phys. Rev. E **47**, 4083 (1993).
[31] L. E. Reich, *A Modern Course in Statistical Physics*, 2nd ed. (Wiley-Interscience Publications, New York, 1998).